Collision cross sections of polyoxometalate anions and determination of Lennard-Jones interaction parameters of Mo and W in He and N_2

*Sébastien Hupin,[1] Vincent Tognetti,[1] Frédéric Rosu,[2] Séverine Renaudineau[3], Anna Proust[3], Guillaume Izzet[3], Valérie Gabelica[4], Carlos Afonso,[1] Hélène Lavanant[1]**

[1] Normandie Univ, UNIROUEN, INSA Rouen, CNRS, COBRA, 76000 Rouen, France

[2] CNRS, University of Bordeaux and INSERM, Institut Européen de Chimie et Biologie (IECB, UMS3033, US001), 2 rue Robert Escarpit, 33600 Pessac, France

[3] Sorbonne Universités, UPMC Univ Paris 06, CNRS UMR 8232, Institut Parisien de Chimie Moléculaire, 4 Place Jussieu, F-75005 Paris, France

[4] University of Bordeaux, INSERM and CNRS, Laboratoire Acides Nucléiques: Régulations Naturelle et Artificielle (ARNA, U1212, UMR5320), site IECB, 2 rue Robert Escarpit, 33600 Pessac, France

Supplementary Information

Table S1. List of the tuning parameters on the Agilent 6560 IMS Q-TOF

Figure S1—S8. Experimental and calculated isotopic distribution of POM anions. Extracted ion mobility at 7.553 V cm^{-1} with different experimental conditions. $^{DT}CCS_{He}$ obtained from the different experimental conditions.

Figure S9 – S21. (a) Linear fit of the drift time *vs* the reciprocal of the electric field for POM anions (b) Residues of the linear fit for data

Figure S22. (a) Superimposed structures of Lindqvist $Mo_6O_{19}^{2-}$ and $W_6O_{19}^{2-}$ anions before and after DFT optimization (b) Superimposed structures of Keggin $PMo_{12}O_{40}^{3-}$ and $PW_{12}O_{40}^{3-}$ anions before and after DFT optimization.

Table S2. Atomic coordinates (Å) and ESP Partial charges for $Mo_6O_{19}^{2-}$ and $W_6O_{19}^{2-}$after DFT optimization

Table S3. Atomic coordinates (Å) and ESP Partial charges for $PMo_{12}O_{40}^{3-}$ and $PW_{12}O_{40}^{3-}$ after DFT optimization.

Figure S23. (a) Collision cross sections calculated with the trajectory method for Lindqvist anions (a) in helium and (b) in N_2 using Lennard Jones ε and σ parameters multiplied by different scaling factors

Figure S24. Points of minimal relative error on the LJ parameters surface: Mo-He data in small light blue diagonal crosses, W-He data in small dark blue vertical crosses, Mo-N_2 data in large light blue diagonal crosses, W-N_2 data in large dark blue vertical crosses.

Table S1(a). List of the tuning parameters applied in the pre-IMS region.

Source: gas temperature	220°C
Source: drying gas	1.5 L/min
Source: Nebulizer pressure	9 psig
Source: capillary	-3500V
Optics 1: FRAGMENTOR	**soft**: -300 V **harsh**: -600 V
IM front funnel: high pressure funnel delta	-110 V
IM front funnel: high pressure funnel RF	100-180 V_{p-p}
IM front funnel: trap funnel delta	-140 V
IM front funnel: trap funnel RF	160 V_{p-p}
IM front funnel: trap funnel exit	-10 V
IM trap: trap entrance grid low	-70 V
IM trap: trap entrance grid delta	-2 V
IM trap: trap entrance	-69 V
IM trap: trap exit	-67 V
IM trap: trap exit grid 1 low	-64 V
IM trap: trap exit grid 1 delta	-5 V
IM trap: trap exit grid 2 low	-63 V
IM trap: trap exit grid 2 delta	-9 V
Acquisition: trap fill time	1000 μs
Acquisition: trap release time	200 μs
IM drift tube: drift tube exit	-210 V

Table S1(b). List of the tuning parameters applied in the post-IMS region.

	Standard POST -IMS	Softer POST-IMS Compromised	Softest POST-IMS Optimized
IM rear funnel: rear funnel entrance	–250V	–200V	–200V
IM rear funnel: rear funnel RF	150 $V_{p–p}$	180 $V_{p–p}$	180 $V_{p–p}$
IM rear funnel: rear funnel exit	–43 V	–35 V	–26 V
IM rear funnel: IM Hex Entrance	–41 V	–32 V	–24 V
IM rear funnel: IM Hex Delta	–9 V	–3 V	–2 V
Optics 1: Oct Entrance Lens	–32 V	–27 V	–21 V
Optics 1: Oct 1 DC	–31.3 V	–25 V	–20 V
Optics 1: Lens 1	–29.4 V	–20 V	–19 V
Optics 1: Lens 2	disabled	disabled	disabled
Quad: Quad DC	–27.8 V	–21 V	–18 V
Quad: PostFilter DC	–27.8 V	–21 V	–17 V
Cell: Gas flow	22 psi	20 psi	20 psi
Cell: Cell Entrance	–26.8 V	–20 V	–16 V
Cell: Hex DC	–25.8 V	–20 V	–16 V
Cell: Hex Delta	9 V	3 V	3 V
Cell: Hex2 DC	–16.6V	–14.6 V	–12V
Cell: Hex2 DV	3 V	1.5 V	1 V
Optics 2: Hex3 DC	–13.2 V	–12.9 V	–11 V
Extractor: Ion focus	–10 V	–10 V	–10 V

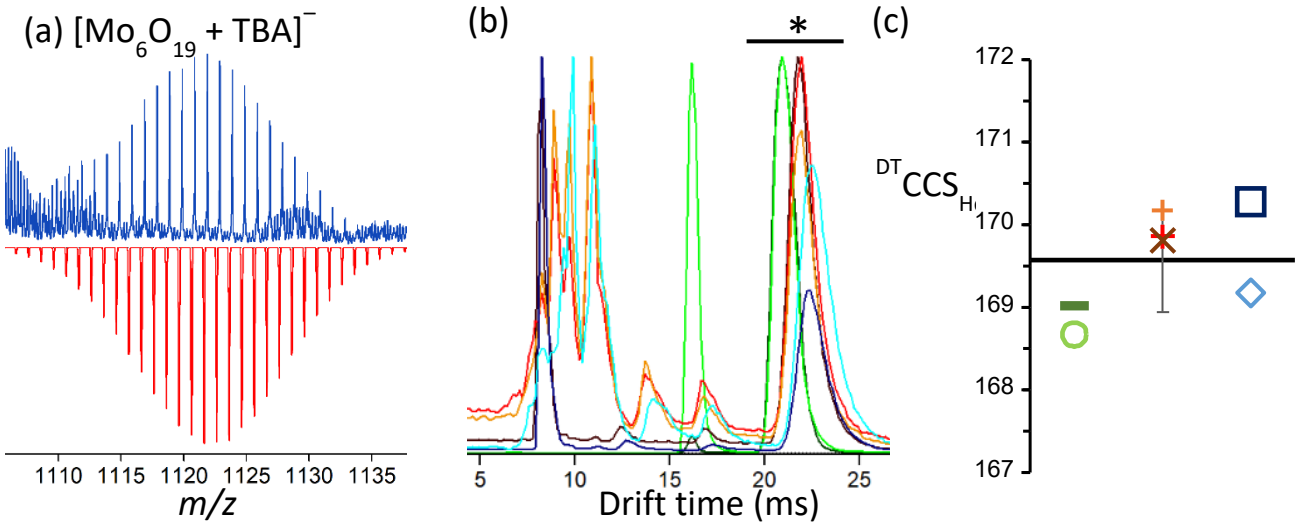

Figure S1. (a) Isotopic distribution of the $[Mo_6O_{19} + TBA]^-$ (*m/z* 1122.04) Lindqvist POM anion with the experimental mass spectrum in blue (soft fragmentor voltage and optimized post IMS tuning) and the calculated distribution in red. (b) Extracted ion mobility spectra for the distribution around *m/z* 1122.04 at 7.553 V cm^{-1} with seven different experimental conditions. Only the peaks labelled with an asterisk were attributed to $[Mo_6O_{19} + TBA]^-$. All other ion mobility signals could not be clearly attributed. (c) $^{DT}CCS_{He}$ of the $[Mo_6O_{19} + TBA]^-$ Lindqvist POM anion obtained from the seven different experimental conditions. The mean value is represented by a back horizontal line and the vertical error bars represent the standard deviation. Legend of experimental conditions in (b) and (c): green: standard post IMS tuning; blue: compromised post IMS tuning; orange, red and brown: optimized post IMS tuning; dark green, brown and dark blue were obtained with harsh fragmentor voltages, and light colors with soft fragmentor voltages.

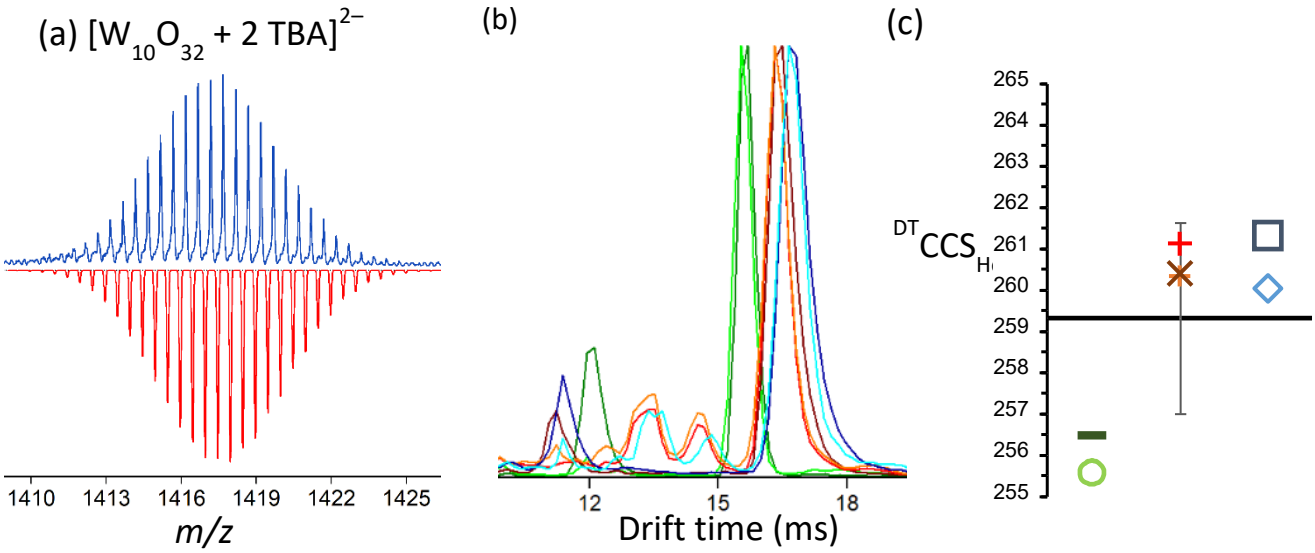

Figure S2. (a) Isotopic distribution of the $[W_{10}O_{32} + 2\ TBA]^{2-}$ (*m/z* 1417.66) decatungstate POM anion with the experimental mass spectrum in blue (soft fragmentor voltage and optimized post IMS tuning) and the calculated distribution in red. (b) Extracted ion mobility spectra for the distribution around *m/z* 1417.66 at 7.553 V cm^{-1} with seven different experimental conditions. Only the intense peaks were attributed to $[W_{10}O_{32} + 2\ TBA]^{2-}$. All other ion mobility signals could not be clearly attributed. (c) $^{DT}CCS_{He}$ of the $[[W_{10}O_{32} + 2\ TBA]^{2-}$ decatungstate POM anions obtained from the seven different experimental conditions. The mean values are represented by a back horizontal line and the vertical error bars represent the standard deviation. Legend of experimental conditions in (b) and (c): green: standard post IMS tuning; blue: compromised post IMS tuning; orange, red and brown: optimized post IMS tuning; dark green, brown and dark blue were obtained with harsh fragmentor voltages, and light colors with soft fragmentor voltages.

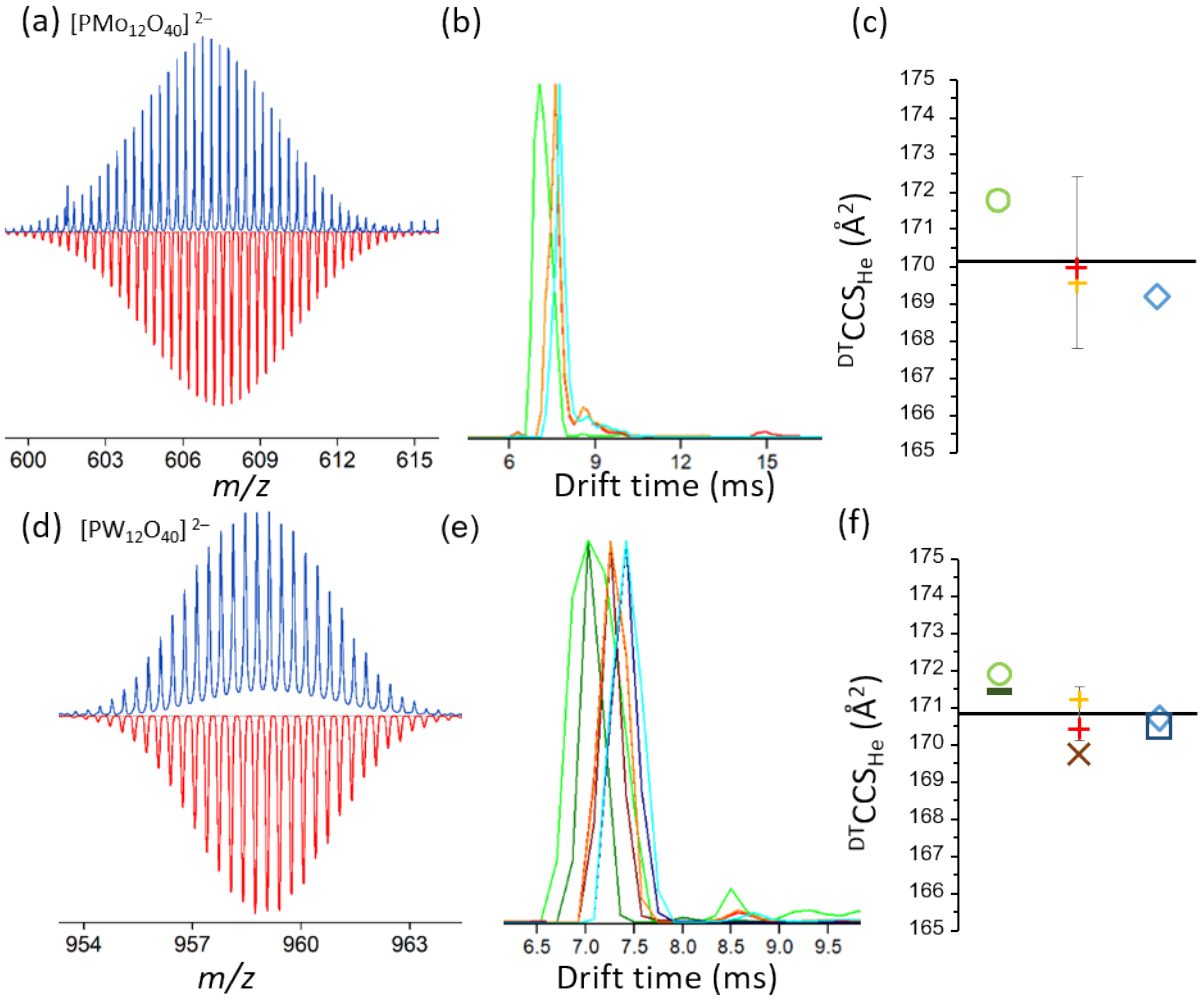

Figure S3. (a) and (d) Isotopic distribution of the $PMo_{12}O_{40}^{2-}$ (*m/z* 607.4) and the $PW_{12}O_{40}^{2-}$ (*m/z* 959.0) Keggin POM anions with the experimental mass spectrum in blue (soft fragmentor voltage and optimized post IMS tuning) and the calculated distribution in red. (b) and (e) Extracted ion mobility spectra for the distribution around *m/z* 607.4 or *m/z* 959.0 at 7.553 V cm^{-1} with five to seven different experimental conditions. (c) and (f) $^{DT}CCS_{He}$ of the $PMo_{12}O_{40}^{2-}$ or the $PW_{12}O_{40}^{2-}$ Keggin POM anions obtained from the five to seven different experimental conditions. The mean values are represented by a back horizontal line and the vertical error bars represent the standard deviation. The $PMo_{12}O_{40}^{2-}$ (*m/z* 607.4) anions were not observed with harsh fragmentor voltages. Legend of experimental conditions in (b), (c), (e) and (f): green: standard post IMS tuning; blue: compromised post IMS tuning; orange, red and brown: optimized post IMS tuning; dark green, brown and dark blue were obtained with harsh fragmentor voltages, and light colors with soft fragmentor voltages.

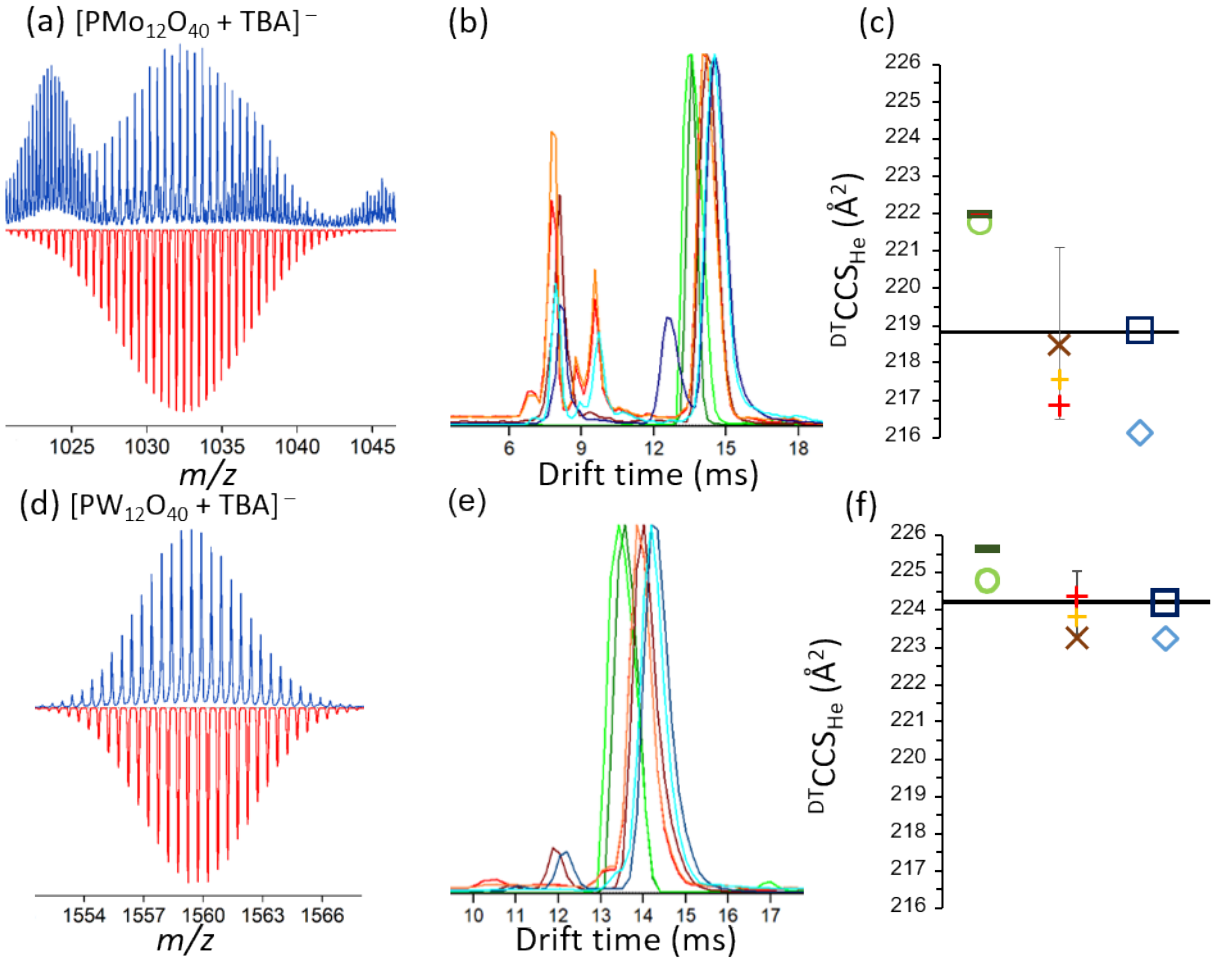

Figure S4. (a) and (d) Isotopic distribution of the $[PMo_{12}O_{40} + TBA]^-$ (*m/z* 1032.3) and the $[PW_{12}O_{40} + TBA]^-$ (*m/z* 1559.8) Keggin POM anions with the experimental mass spectrum in blue (soft fragmentor voltage and optimized post IMS tuning) and the calculated distribution in red. (b) and (e) Extracted ion mobility spectra for the distribution around *m/z* 1032.3 or *m/z* 1559.8 at 7.553 V cm^{-1} with seven different experimental conditions. (c) and (f) $^{DT}CCS_{He}$ of the $[PMo_{12}O_{40} + TBA]^-$ or the $[PW_{12}O_{40} + TBA]^-$ Keggin POM anions obtained from the seven different experimental conditions. The mean values are represented by a back horizontal line and the vertical error bars represent the standard deviation. Legend of experimental conditions in (b), (c), (e) and (f): green: standard post IMS tuning; blue: compromised post IMS tuning; orange, red and brown: optimized post IMS tuning; dark green, brown and dark blue were obtained with harsh fragmentor voltages, and light colors with soft fragmentor voltages.

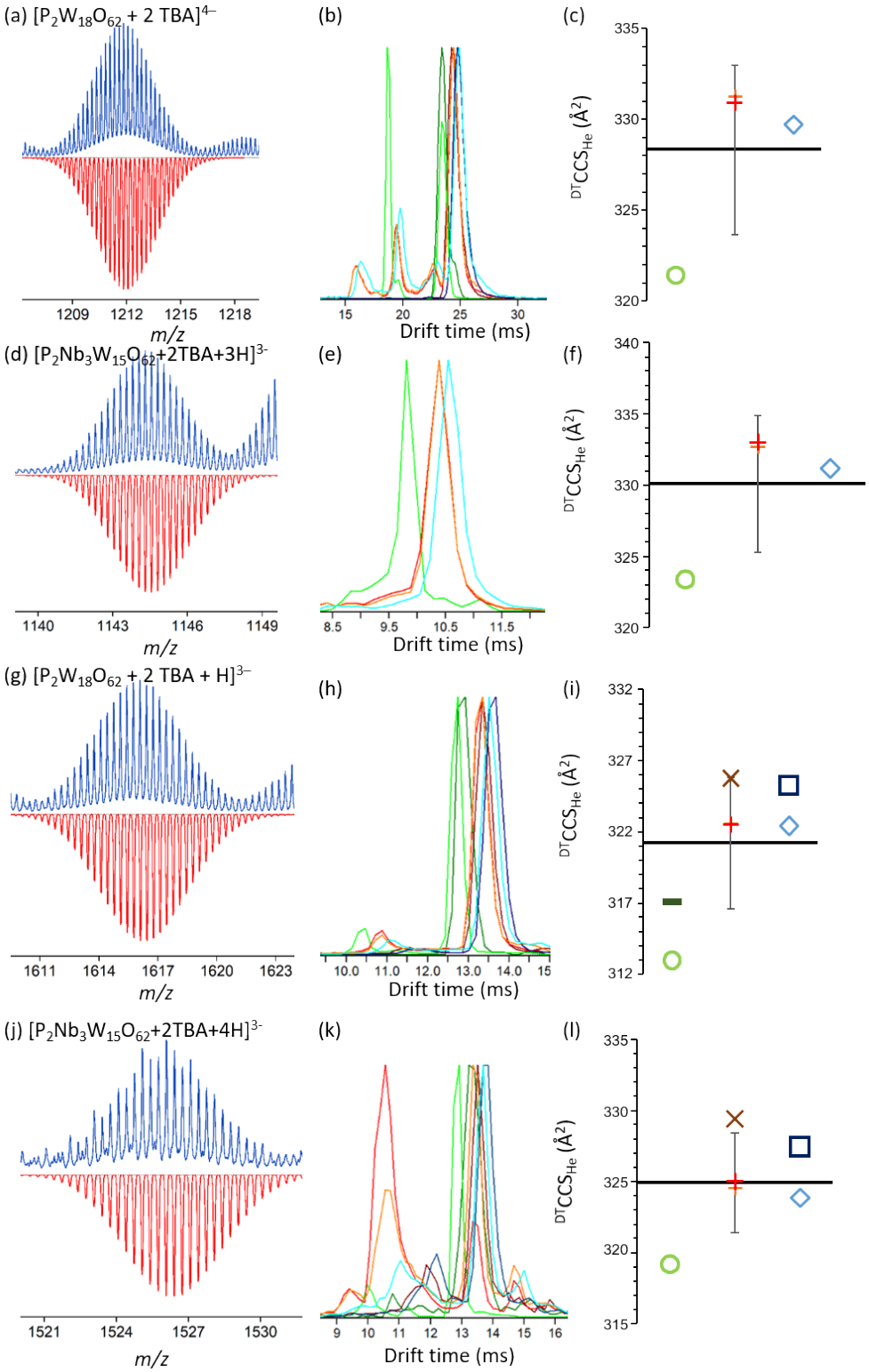

Figure S5. (a) (d) (g) (j) Isotopic distribution of the Dawson POM anions with 2 TBA counter ions with the experimental mass spectrum in blue (soft fragmentor voltage and optimized post IMS tuning) and the calculated distribution in red. (b) (e) (h) (k) Extracted ion mobility spectra at 7.553 V cm^{-1} with four to seven different experimental conditions. (c) (f) (i) (l) $^{DT}CCS_{He}$ of the Dawson POM anions with 2 TBA counter ions obtained from the different experimental conditions. The mean values are represented by a back horizontal line and the vertical error bars represent the standard deviation. Legend of experimental conditions: green: standard post IMS tuning; blue: compromised post IMS tuning; orange, red and brown: optimized post IMS tuning; dark green, brown and dark blue were obtained with harsh fragmentor voltages, and light colors with soft fragmentor voltages.

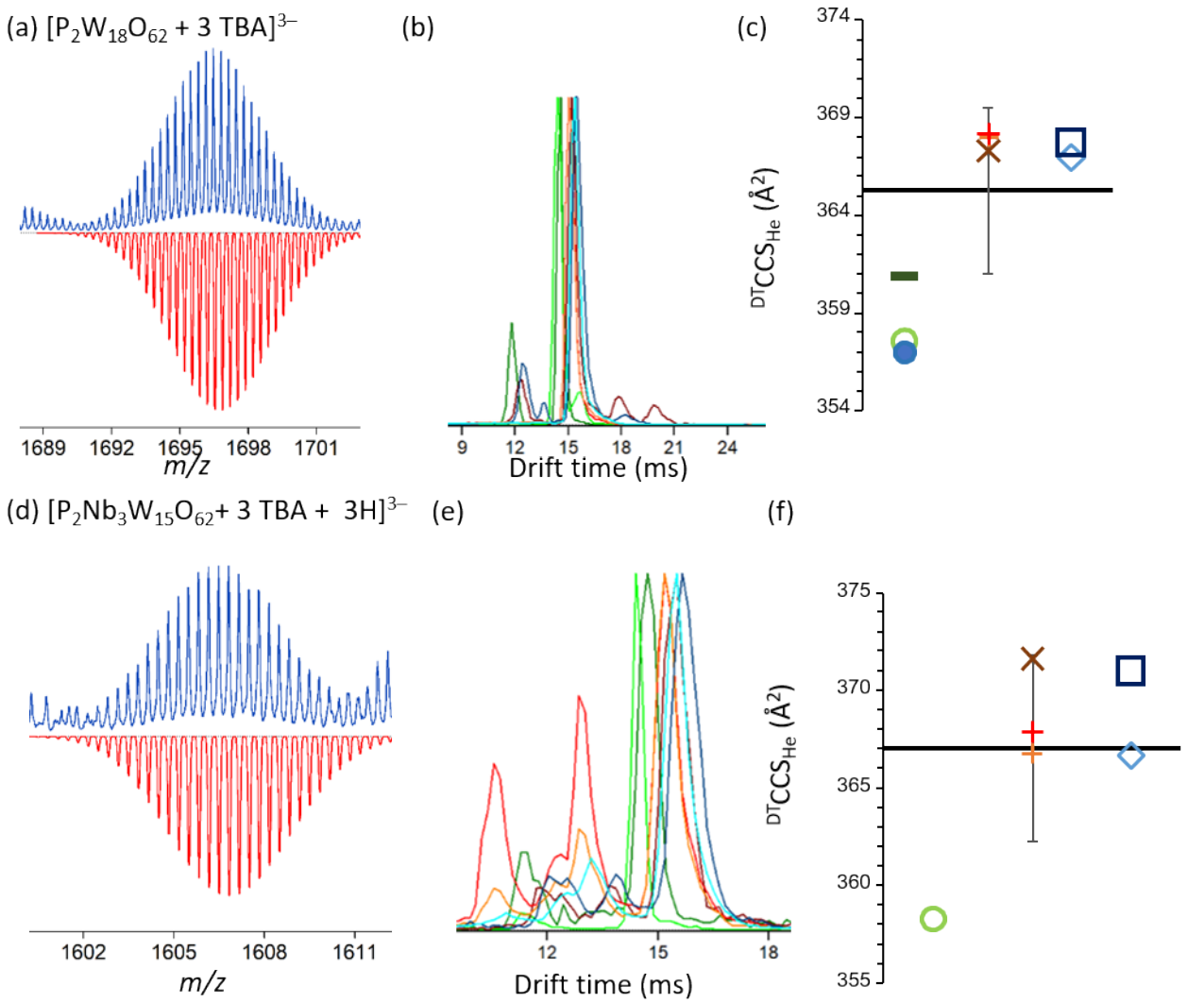

F

igure S6. (a) and (d) Isotopic distribution of the $[P_2W_{18}O_{62}$ + 3 TBA$]^-$ (*m/z* 1696.8) and the $[P_2Nb_3W_{15}O_{62}$+3TBA+3H$]^{3-}$ (*m/z* 1606.9) Dawson POM anions with the experimental mass spectrum in blue (soft fragmentor voltage and optimized post IMS tuning) and the calculated distribution in red. (b) and (e) Extracted ion mobility spectra for the distribution around *m/z* 1696.8 or *m/z* 1606.9 at 7.553 V cm^{-1} with seven different experimental conditions. Only the intense peaks were attributed to $[P_2Nb_3W_{15}O_{62}$+3TBA+3H$]^{3-}$. All other ion mobility signals could not be clearly attributed. (c) and (f) $^{DT}CCS_{He}$ of the $[PMo_{12}O_{40}$ + TBA$]^-$ or the $[PW_{12}O_{40}$ + TBA$]^-$ Dawson POM anions obtained from the seven different experimental conditions. The mean values are represented by a back horizontal line and the vertical error bars represent the standard deviation. The blue dot is the value published in Surman *et al* (*J. Am. Chem. Soc.* 2016). Legend of experimental conditions in (b), (c), (e) and (f): green: standard post IMS tuning; blue: compromised post IMS tuning; orange, red and brown: optimized post IMS tuning; dark green, brown and dark blue were obtained with harsh fragmentor voltages, and light colors with soft fragmentor voltages.

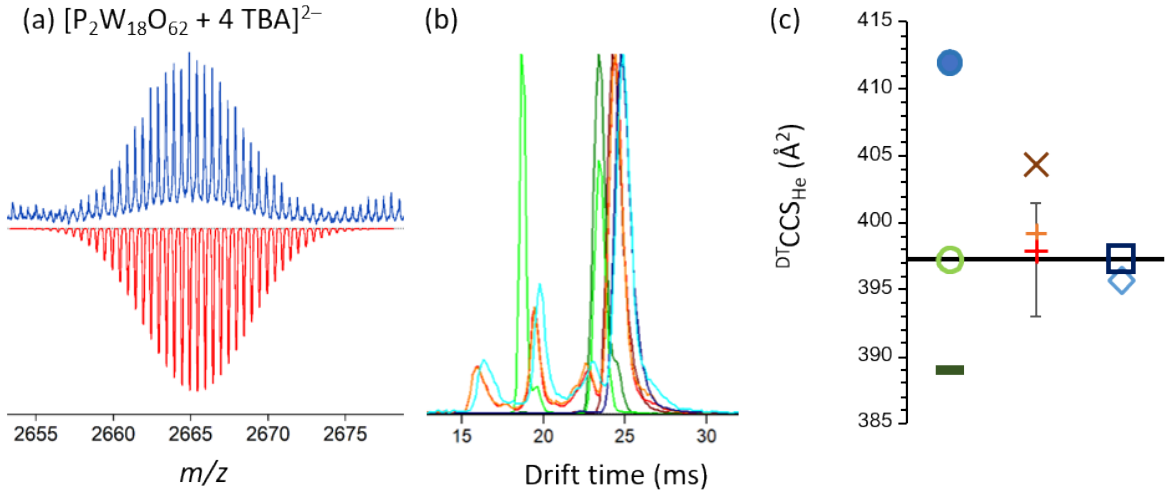

Figure S7. (a) Isotopic distribution of the $[P_2W_{18}O_{62} + 4\ TBA]^{2-}$ (*m/z* 2666.5) Dawson POM anion with the experimental mass spectrum in blue (soft fragmentor voltage and optimized post IMS tuning) and the calculated distribution in red. (b) Extracted ion mobility spectra for the distribution around *m/z* 2666 at 7.553 V cm^{-1} with seven different experimental conditions (c) $^{DT}CCS_{He}$ of the $[P_2W_{18}O_{62} + 4\ TBA]^{2-}$ Dawson POM anion obtained from the seven different experimental conditions. The mean values are represented by a back horizontal line and the vertical error bars represent the standard deviation. The blue dot is the value published in Surman *et al* (*J. Am. Chem. Soc.* 2016). Legend of experimental conditions in (b) and (c): green: standard post IMS tuning; blue: compromised post IMS tuning; orange, red and brown: optimized post IMS tuning; dark green, brown and dark blue were obtained with harsh fragmentor voltages, and light colors with soft fragmentor voltages.

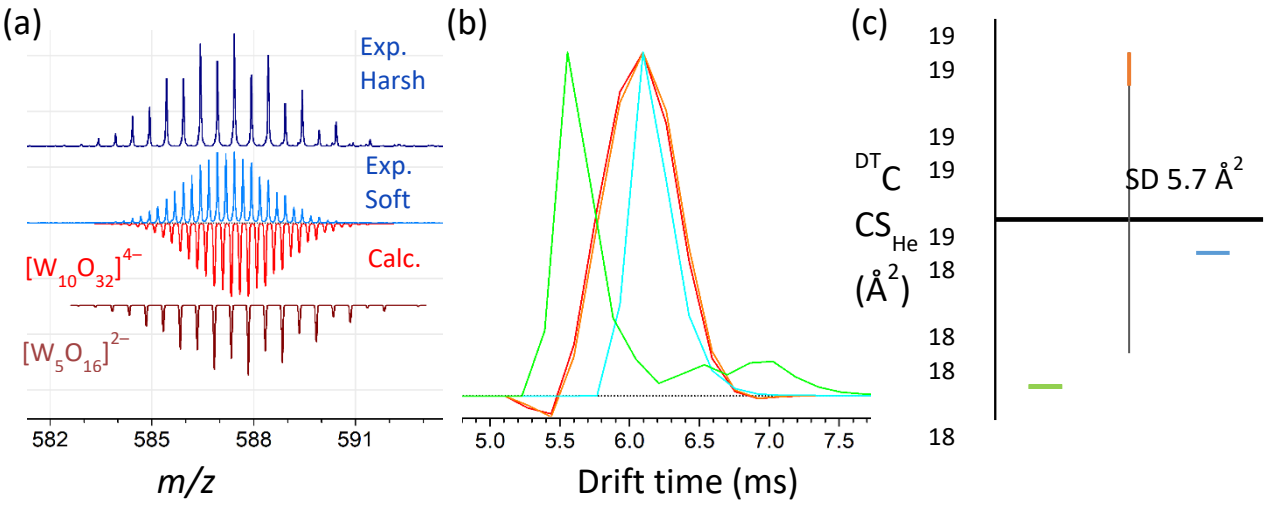

Figure S8. (a) Isotopic distributions around *m/z* 587.6 in two experimental mass spectra obtained with low fragmentor voltage (light blue) and high fragmentor voltage (dark blue). The calculated distribution for $[W_{10}O_{32}]^{4-}$ and $[W_5O_{16}]^{2-}$ are shown below in red and brown respectively. (b) Extracted ion mobility spectra for the distribution around *m/z* 587.6 at 7.553 V cm^{-1} with four different experimental conditions (c) $^{DT}CCS_{He}$ of the $[W_{10}O_{32}]^{4-}$ decatungstate POM anion obtained from the four different experimental conditions. The mean values are represented by a back horizontal line and the vertical error bars represent the standard deviation. Legend of experimental conditions in (b) and (c): green: standard post IMS tuning; blue: compromised post IMS tuning; orange and red: optimized post IMS tuning; only data obtained with soft fragmentor voltages is shown.

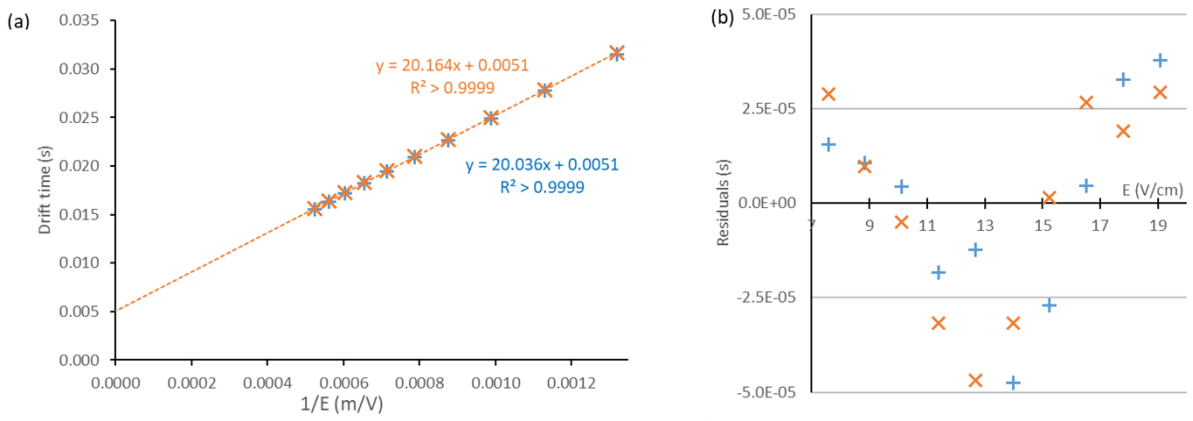

Figure S9. (a) Linear fit of the drift time *vs* the reciprocal of the electric field for $[W_6O_{19}]^{2-}$ (b) Residuals of the linear fit for data obtained from $[W_6O_{19}]^{2-}$. Soft fragmentor voltage: orange diagonal crosses and harsh fragmentor voltage: blue vertical crosses.

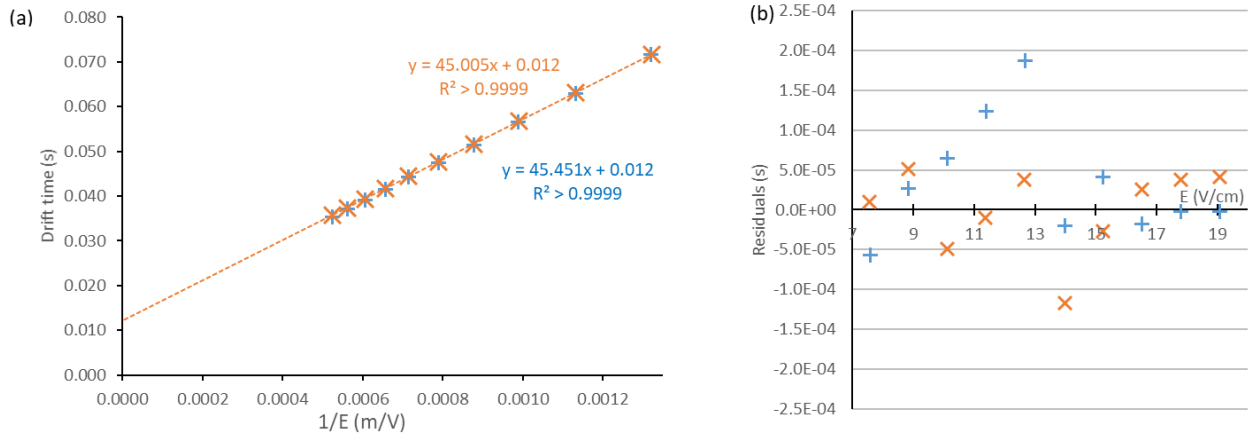

Figure S10. (a) Linear fit of the drift time *vs* the reciprocal of the electric field for $[Mo_6O_{19} + TBA]^{2-}$ (b) Residuals of the linear fit for data obtained from $[Mo_6O_{19} + TBA]^{2-}$. Soft fragmentor voltage: orange diagonal crosses and harsh fragmentor voltage: blue vertical crosses.

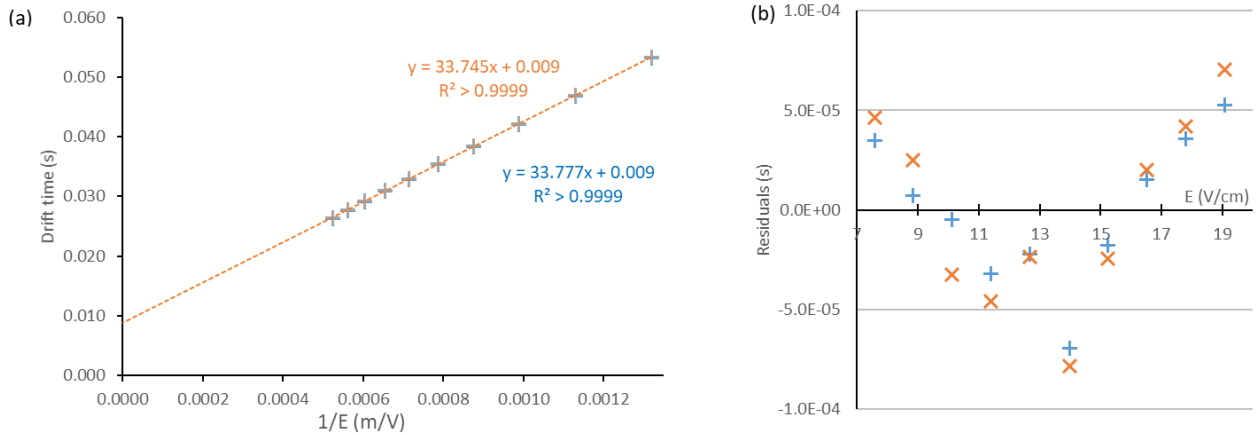

Figure S11. (a) Linear fit of the drift time *vs* the reciprocal of the electric field for $[W_{10}O_{32} + 2\ TBA]^{2-}$ (b) Residues of the linear fit for data obtained from $[W_{10}O_{32} + 2\ TBA]^{2-}$. Soft fragmentor voltage: orange diagonal crosses and harsh fragmentor voltage: blue vertical crosses.

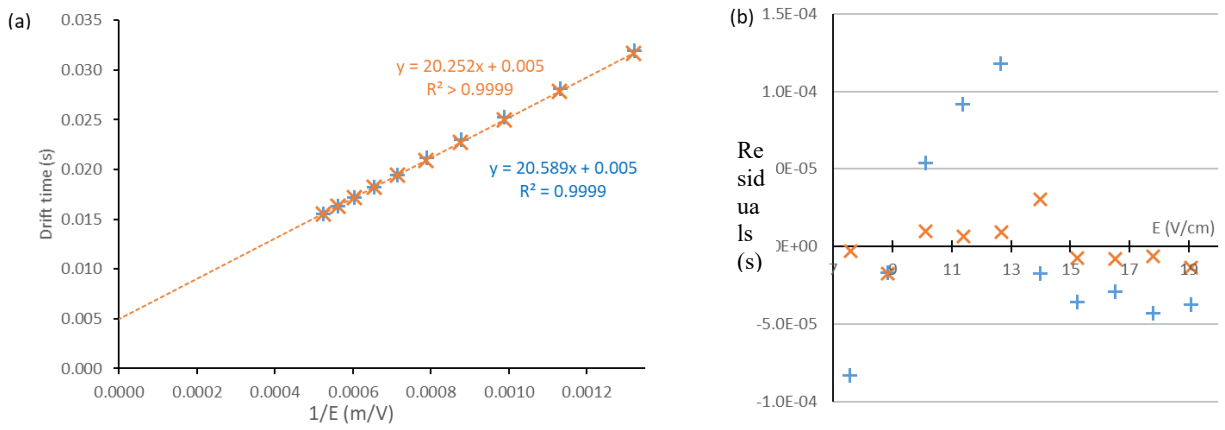

Figure S12. (a) Linear fit of the drift time *vs* the reciprocal of the electric field for $[PMo_{12}O_{40}]^{2-}$ (b) Residuals of the linear fit for data obtained from $[PMo_{12}O_{40}]^{2-}$. Soft fragmentor voltage: orange diagonal crosses and harsh fragmentor voltage: blue vertical crosses.

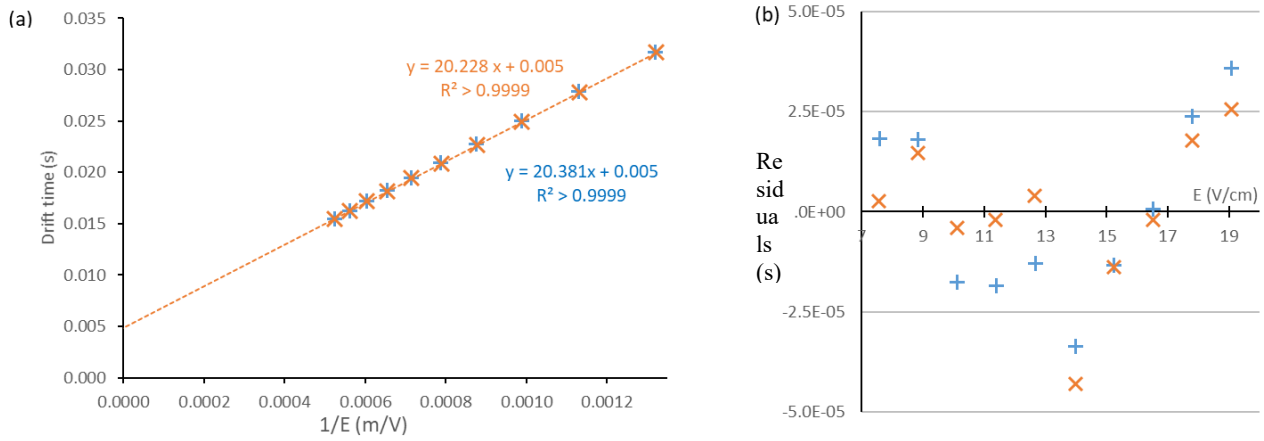

Figure S13. (a) Linear fit of the drift time *vs* the reciprocal of the electric field for $[PW_{12}O_{40}]^{2-}$ (b) Residuals of the linear fit for data obtained from $[PW_{12}O_{40}]^{2-}$. Soft fragmentor voltage: orange diagonal crosses and harsh fragmentor voltage: blue vertical crosses.

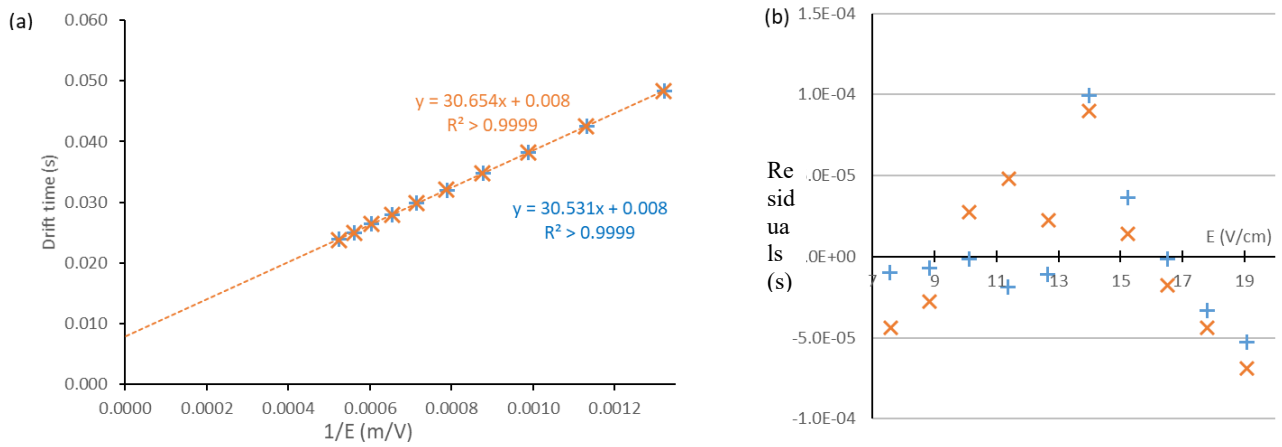

Figure S14. (a) Linear fit of the drift time *vs* the reciprocal of the electric field for $[PMo_{12}O_{40} + TBA]^{2-}$ (b) Residuals of the linear fit for data obtained from $[PMo_{12}O_{40} + TBA]^{2-}$. Soft fragmentor voltage: orange diagonal crosses and harsh fragmentor voltage: blue vertical crosses.

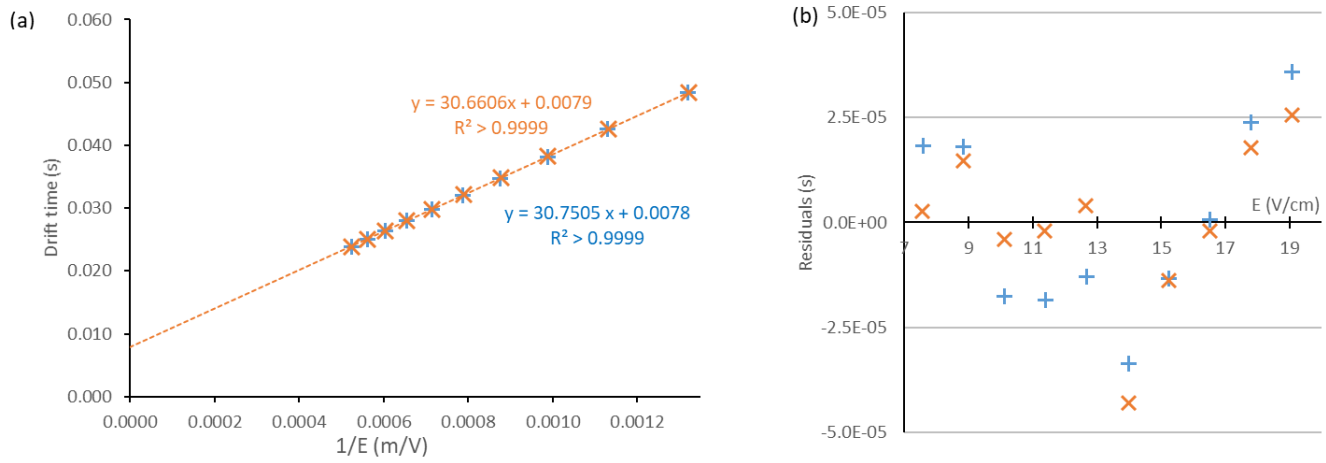

Figure S15. (a) Linear fit of the drift time *vs* the reciprocal of the electric field for $[PW_{12}O_{40} + TBA]^{2-}$ (b) Residuals of the linear fit for data obtained from $[PW_{12}O_{40} + TBA]^{2-}$. Soft fragmentor voltage: orange diagonal crosses and harsh fragmentor voltage: blue vertical crosses.

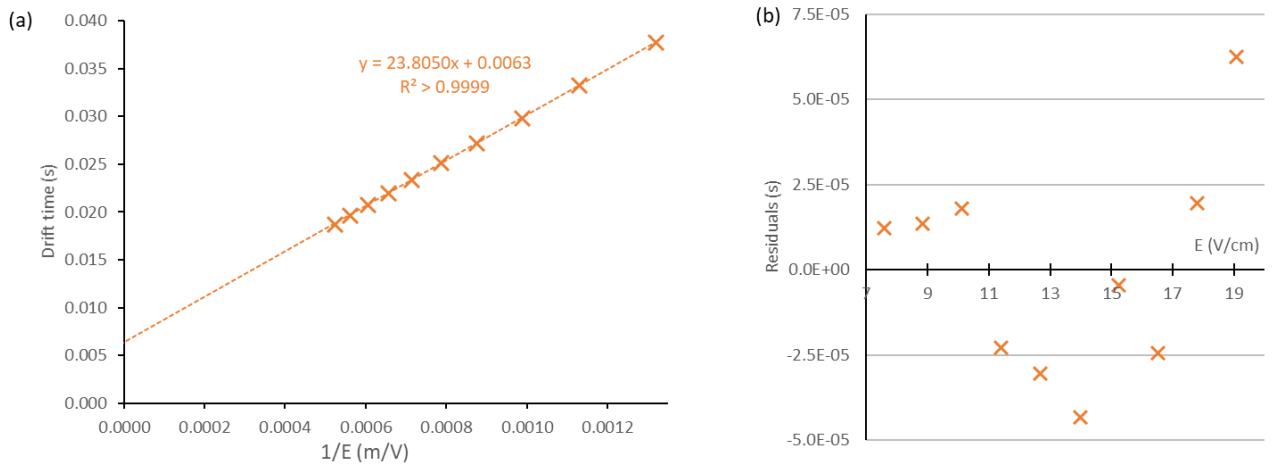

Figure S15. (a) Linear fit of the drift time *vs* the reciprocal of the electric field for $[P_2W_{18}O_{62} + 2\ TBA]^{4-}$ (b) Residuals of the linear fit for data obtained from $[P_2W_{18}O_{62} + 2\ TBA]^{4-}$. $[P_2W_{18}O_{62} + 2\ TBA]^{4-}$ was observed with soft fragmentor voltage only.

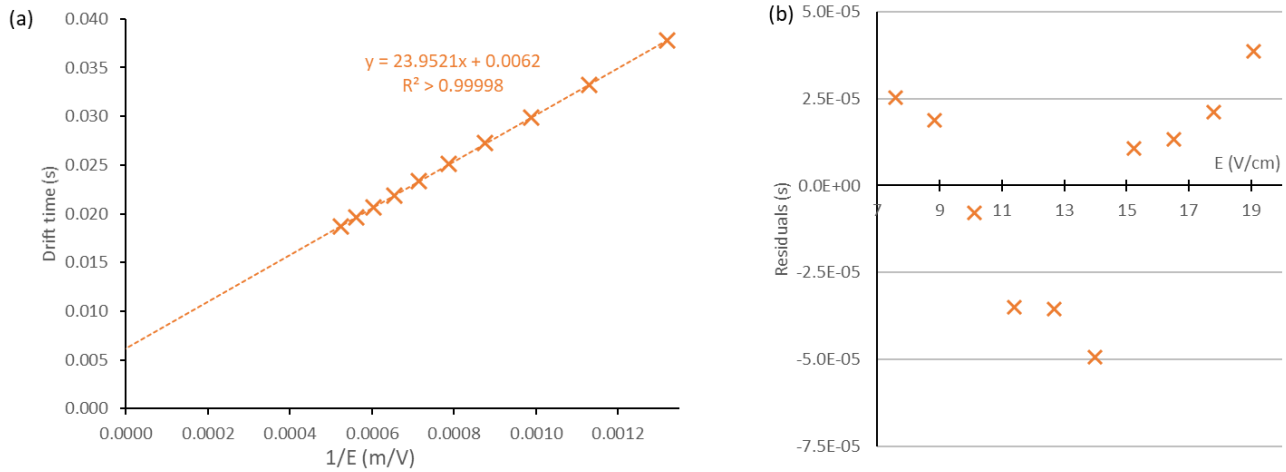

Figure S16. (a) Linear fit of the drift time *vs* the reciprocal of the electric field for $[P_2Nb_3W_{15}O_{62} + 2\ TBA + 3\ H]^{4-}$ (b) Residuals of the linear fit for data obtained from $[P_2Nb_3W_{15}O_{62} + 2\ TBA + 3\ H]^{4-}$which was observed with soft fragmentor voltage only.

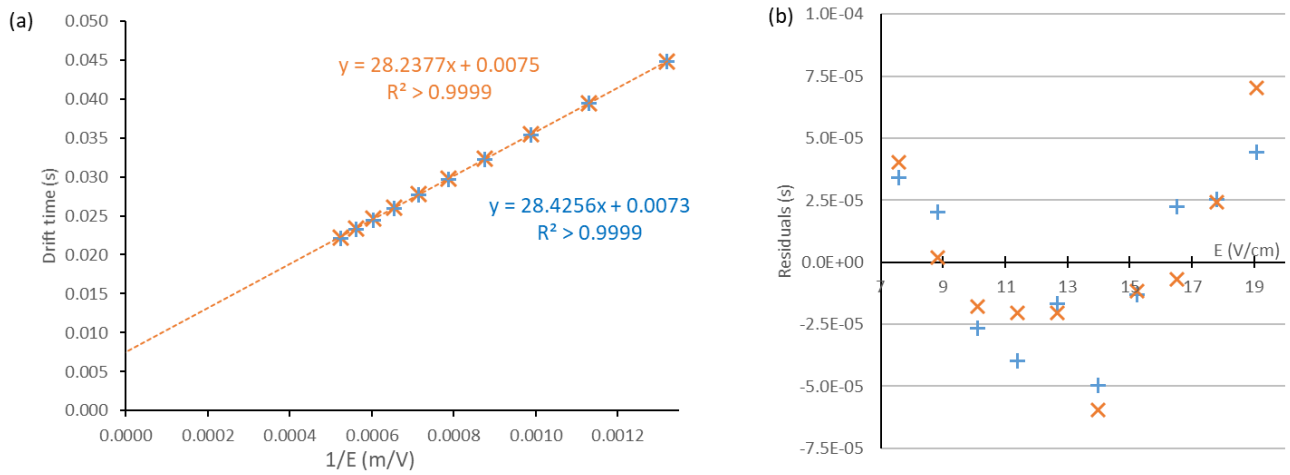

Figure S17. (a) Linear fit of the drift time *vs* the reciprocal of the electric field for $[P_2W_{18}O_{62} + 2\ TBA + H]^{3-}$ (b) Residuals of the linear fit for data obtained from $[P_2W_{18}O_{62} + 2\ TBA + H]^{3-}$. Soft fragmentor voltage: orange diagonal crosses and harsh fragmentor voltage: blue vertical crosses.

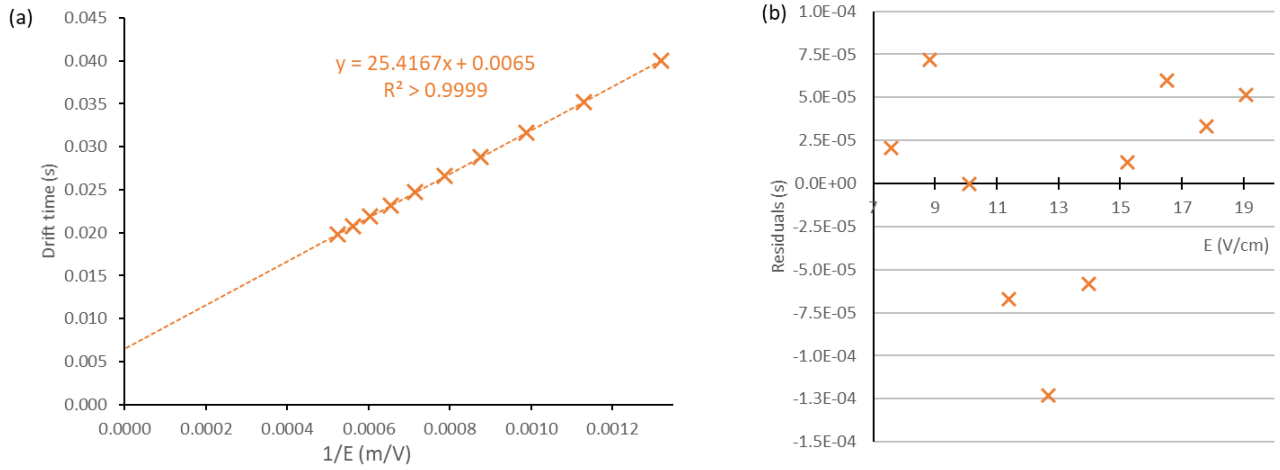

Figure S18. (a) Linear fit of the drift time *vs* the reciprocal of the electric field for $[P_2Nb_3W_{15}O_{62} + 2\ TBA + 4\ H]^{3-}$ (b) Residuals of the linear fit for data obtained from $[P_2Nb_3W_{15}O_{62} + 2\ TBA + 4\ H]^{3-}$. $[P_2Nb_3W_{15}O_{62} + 2\ TBA + 4\ H]^{3-}$ was observed with soft fragmentor voltage only.

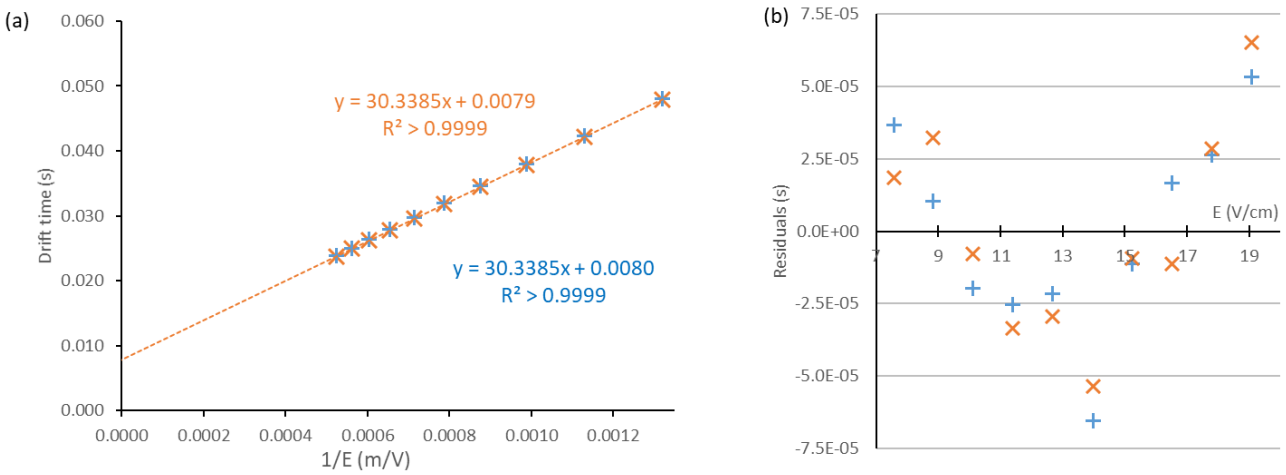

Figure S19. (a) Linear fit of the drift time *vs* the reciprocal of the electric field for $[P_2W_{18}O_{62} + 3\ TBA]^{3-}$ (b) Residuals of the linear fit for data obtained from $[P_2W_{18}O_{62} + 3\ TBA]^{3-}$. Soft fragmentor voltage: orange diagonal crosses and harsh fragmentor voltage: blue vertical crosses.

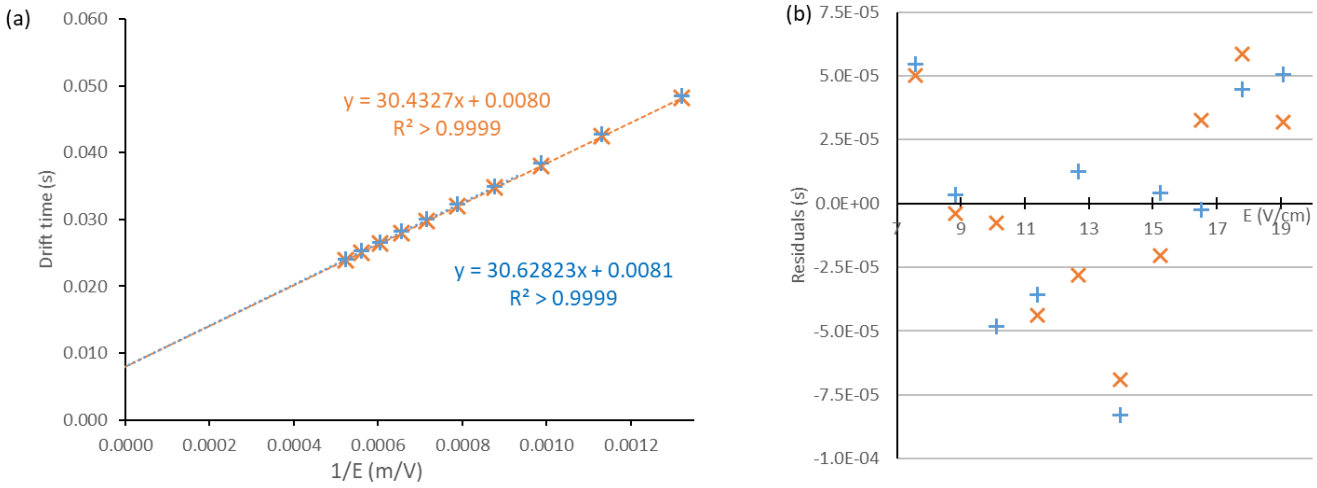

Figure S20. (a) Linear fit of the drift time *vs* the reciprocal of the electric field for $[P_2Nb_3W_{15}O_{62} + 3\ TBA + 3\ H]^{3-}$ (b) Residuals of the linear fit for data obtained from $[P_2Nb_3W_{15}O_{62} + 3\ TBA + 3\ H]^{3-}$. Soft fragmentor voltage: orange diagonal crosses and harsh fragmentor voltage: blue vertical crosses.

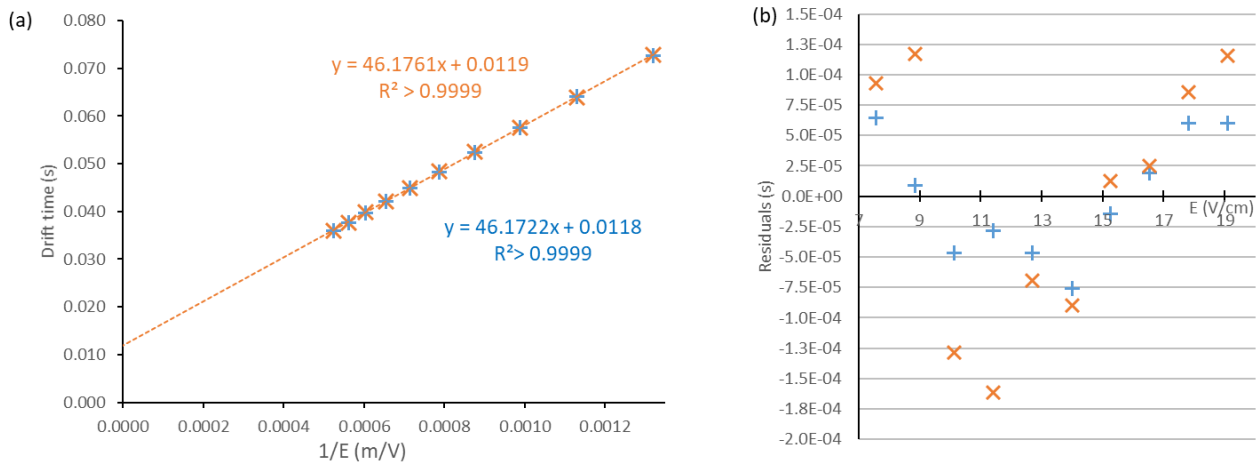

Figure S21. (a) Linear fit of the drift time *vs* the reciprocal of the electric field for $[P_2W_{18}O_{62} + 4\ TBA]^{2-}$ (b) Residuals of the linear fit for data obtained from $[P_2W_{18}O_{62} + 4\ TBA]^{2-}$. Soft fragmentor voltage: orange diagonal crosses and harsh fragmentor voltage: blue vertical crosses.

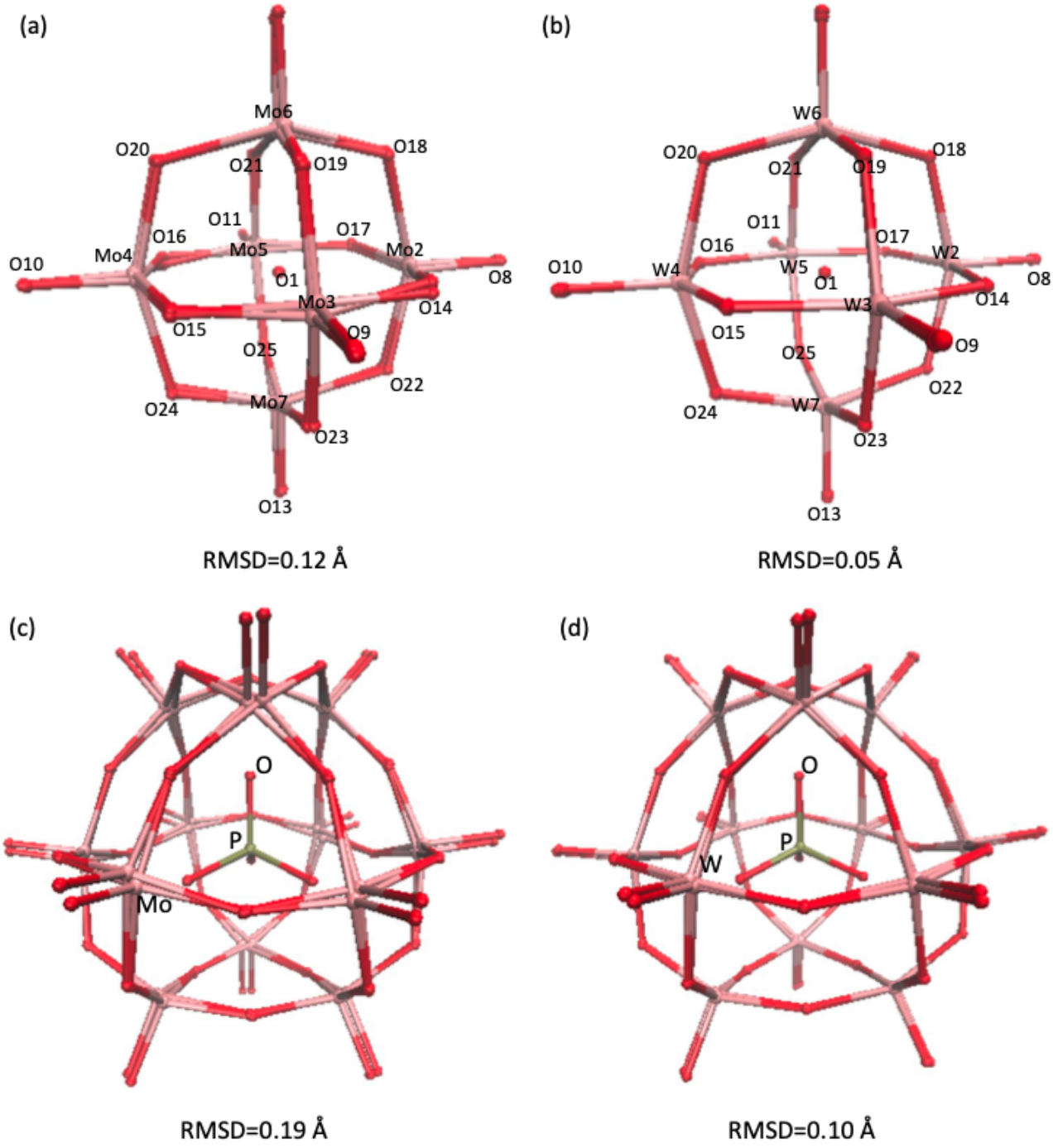

Figure S22a. Superimposed structures comparing X-ray diffraction and DFT optimized geometries of the following anions: (a) Lindqvist $Mo_6O_{19}^{2-}$, (b) Lindqvist $W_6O_{19}^{2-}$, (c) Keggin $PMo_{12}O_{40}^{3-}$, (d) Keggin $PW_{12}O_{40}^{3-}$. Note that some labels are omitted for clarity. Structural root mean square deviation (RMSD) values were computed using the Kabsch alignment algorithm implemented in the VMD software (Humphrey. W., Dalke. A, and Schulten. K. *J. Molec. Graphics* **1996,** *14*, 33-38), which was also used to generate these figures.

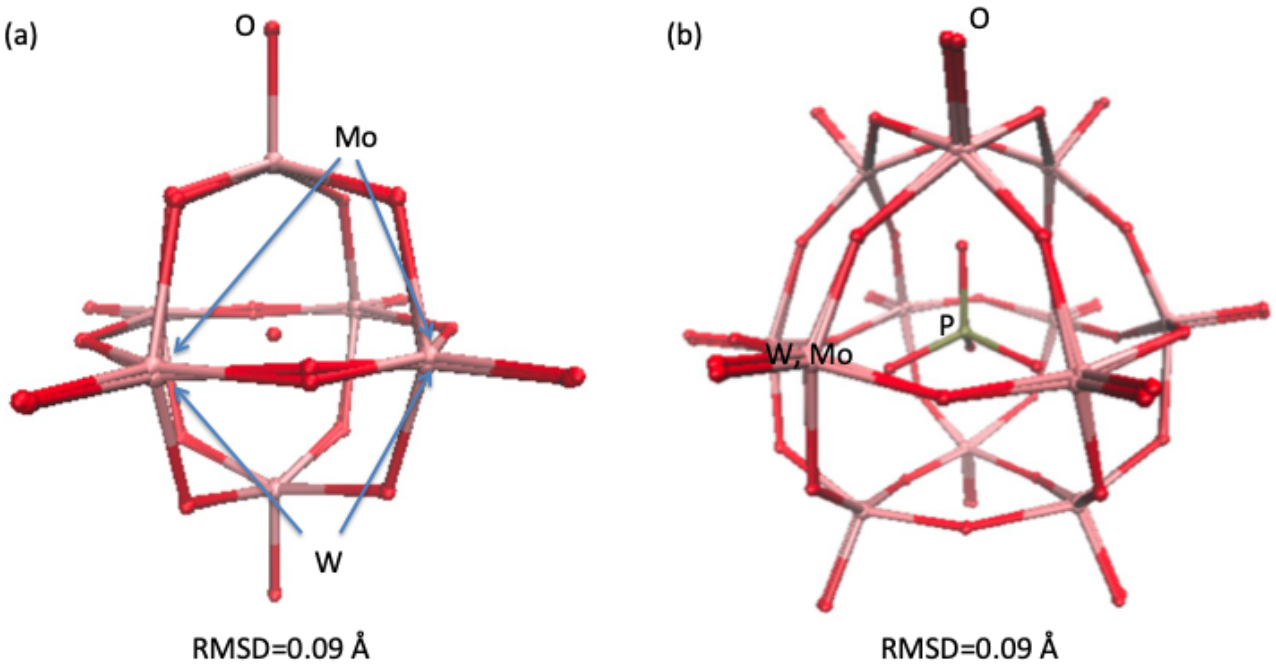

Figure S22b. Superimposed optimized DFT geometries of (a) Lindqvist $Mo_6O_{19}^{2-}$ and Lindqvist $W_6O_{19}^{2-}$ anions, (b) Keggin $PMo_{12}O_{40}^{3-}$ and Keggin $PW_{12}O_{40}^{3-}$ anions. Note that most labels are omitted for clarity. Structural root mean square deviation (RMSD) values were computed using the Kabsch alignment algorithm implemented in the VMD software (Humphrey. W., Dalke. A, and Schulten. K. *J. Molec. Graphics* **1996**, *14*, 33-38), which was also used to generate these figures.

Table S2. Atomic nuclei coordinates (Å) and HLYGAt ESP atomic charges (e) for $Mo_6O_{19}^{2-}$ and $W_6O_{19}^{2-}$ after DFT optimization. Non-bridging oxygen atoms are numbered from 8 to 13. Bridging oxygen atoms are numbered 14 to 25. The central oxygen atom is number 1. The reported Cartesian coordinates are those obtained after structure alignment.

	Atom	X	Y	Z	HLYGAt	Atom	X	Y	Z	HLYGAt
1	O	0.000	0.000	0.000	-0.23	O	0.000	0.000	0.000	-0.79
2	Mo	0.134	-2.023	1.181	1.51	W	0.029	-2.035	1.207	1.79
3	Mo	0.210	-1.180	-2.010	1.52	W	0.114	-1.204	-2.032	1.80
4	Mo	-0.134	2.024	-1.181	1.51	W	-0.028	2.035	-1.207	1.79
5	Mo	-0.210	1.179	2.009	1.52	W	-0.114	1.204	2.033	1.80
6	Mo	-2.372	-0.216	-0.109	1.50	W	-2.362	-0.082	-0.084	1.79
7	Mo	2.372	0.217	0.109	1.50	W	2.363	0.082	0.085	1.79
8	O	0.073	-3.479	2.041	-0.51	O	0.044	-3.509	2.078	-0.58
9	O	0.221	-2.050	-3.461	-0.51	O	0.191	-2.072	-3.506	-0.58
10	O	-0.073	3.479	-2.041	-0.51	O	-0.043	3.509	-2.078	-0.58
11	O	-0.219	2.050	3.460	-0.51	O	-0.191	2.072	3.506	-0.58
12	O	-4.064	-0.185	-0.154	-0.52	O	-4.073	-0.135	-0.146	-0.58
13	O	4.064	0.185	0.152	-0.52	O	4.073	0.135	0.146	-0.58
14	O	-0.038	-2.550	-0.653	-0.67	O	0.097	-2.571	-0.661	-0.71
15	O	0.078	0.654	-2.545	-0.67	O	0.071	0.665	-2.571	-0.71
16	O	0.038	2.551	0.653	-0.67	O	-0.097	2.571	0.661	-0.71
17	O	-0.078	-0.655	2.546	-0.67	O	-0.071	-0.665	2.571	-0.71
18	O	-1.924	-1.622	0.945	-0.64	O	-1.859	-1.676	0.888	-0.71
19	O	-1.842	-0.942	-1.695	-0.64	O	-1.790	-1.005	-1.686	-0.71
20	O	-1.895	1.630	-0.992	-0.63	O	-1.893	1.563	-1.016	-0.71
21	O	-1.962	0.986	1.533	-0.64	O	-1.963	0.895	1.549	-0.71
22	O	1.895	-1.631	0.992	-0.63	O	1.893	-1.563	1.016	-0.71
23	O	1.961	-0.986	-1.532	-0.64	O	1.963	-0.895	-1.549	-0.71
24	O	1.924	1.623	-0.945	-0.64	O	1.859	1.676	-0.888	-0.71
25	O	1.844	0.942	1.696	-0.64	O	1.790	1.005	1.686	-0.71

Table S3. Atomic nuclei coordinates (Å) and HLYGAt ESP atomic charges (e) for $PMo_{12}O_{40}^{3-}$ and $PW_{12}O_{40}^{3-}$ after DFT optimization. Non-bridging oxygen atoms are numbered from 18 to 29. Atoms 14 to 17 are oxygen atoms bridging the central phosphorus atom with a metal atom. Atoms 30 to 53 are oxygen atoms bridging two metal atoms. The reported Cartesian coordinates are those obtained after structure alignment.

	Atom	X	Y	Z	HLYGAt	Atom	X	Y	Z	HLYGAt
1	P	0.000	0.000	0.000	2.04	P	0.000	0.000	0.000	2.90
2	Mo	-3.194	-0.985	1.318	1.36	W	-3.142	-1.018	1.447	1.56
3	Mo	-1.970	-2.605	-1.498	1.36	W	-2.087	-2.523	-1.505	1.56
4	Mo	1.055	-1.207	-3.215	1.36	W	1.040	-1.344	-3.180	1.57
5	Mo	3.217	0.800	-1.386	1.36	W	3.162	0.846	-1.511	1.57
6	Mo	1.920	2.533	1.676	1.37	W	2.042	2.455	1.672	1.57
7	Mo	-0.864	1.210	3.270	1.37	W	-0.862	1.348	3.231	1.57
8	Mo	-0.515	-3.174	1.601	1.36	W	-0.474	-3.250	1.487	1.56
9	Mo	2.594	-2.458	-0.367	1.36	W	2.692	-2.379	-0.300	1.57
10	Mo	1.999	-0.715	2.899	1.37	W	1.889	-0.764	2.976	1.57
11	Mo	-2.022	0.899	-2.830	1.37	W	-1.909	0.936	-2.911	1.56
12	Mo	0.325	3.171	-1.656	1.37	W	0.296	3.248	-1.537	1.57
13	Mo	-2.544	2.531	0.188	1.37	W	-2.646	2.446	0.133	1.57
14	O	-0.733	1.143	-0.744	-0.42	O	-0.733	1.139	-0.743	-0.64
15	O	-0.984	-1.171	0.246	-0.42	O	-0.981	-1.169	0.246	-0.62
16	O	1.188	-0.498	-0.861	-0.40	O	1.186	-0.495	-0.858	-0.64
17	O	0.529	0.523	1.357	-0.41	O	0.528	0.522	1.355	-0.64
18	O	-4.654	-1.156	2.143	-0.47	O	-4.628	-1.195	2.264	-0.52
19	O	-2.887	-3.613	-2.489	-0.47	O	-3.004	-3.558	-2.503	-0.52
20	O	1.210	-1.878	-4.753	-0.47	O	1.204	-2.010	-4.741	-0.52
21	O	4.610	1.513	-2.010	-0.47	O	4.582	1.559	-2.131	-0.52
22	O	2.985	3.752	2.146	-0.47	O	3.104	3.699	2.154	-0.52
23	O	-1.578	1.872	4.645	-0.47	O	-1.579	2.005	4.632	-0.53
24	O	-3.878	3.503	0.527	-0.47	O	-3.985	3.444	0.476	-0.53
25	O	-2.820	1.033	-4.308	-0.47	O	-2.732	1.074	-4.399	-0.52
26	O	0.769	4.693	-2.228	-0.47	O	0.744	4.782	-2.131	-0.53
27	O	-0.399	-4.688	2.333	-0.47	O	-0.369	-4.775	2.241	-0.52
28	O	3.781	-3.641	-0.183	-0.47	O	3.884	-3.586	-0.127	-0.53
29	O	2.863	-1.392	4.177	-0.47	O	2.777	-1.439	4.265	-0.52
30	O	-3.427	-2.008	-0.177	-0.58	O	-3.423	-1.988	-0.151	-0.64
31	O	-0.416	-2.381	-2.409	-0.60	O	-0.442	-2.386	-2.409	-0.68
32	O	2.501	-0.096	-3.089	-0.58	O	2.475	-0.115	-3.094	-0.64
33	O	3.025	1.562	0.250	-0.60	O	3.035	1.562	0.224	-0.68
34	O	0.602	2.608	2.938	-0.58	O	0.624	2.609	2.915	-0.64
35	O	-2.035	-0.070	2.737	-0.60	O	-2.032	-0.046	2.752	-0.68
36	O	-3.300	0.664	0.570	-0.60	O	-3.308	0.647	0.589	-0.68
37	O	-2.461	-0.759	-2.240	-0.60	O	-2.457	-0.741	-2.261	-0.68
38	O	-0.256	0.032	-3.404	-0.60	O	-0.244	0.010	-3.413	-0.68
39	O	1.781	2.136	-1.976	-0.60	O	1.770	2.160	-1.971	-0.68
40	O	1.025	3.246	0.267	-0.60	O	1.046	3.243	0.283	-0.68
41	O	-1.713	2.346	1.791	-0.60	O	-1.736	2.350	1.777	-0.68
42	O	-3.049	1.902	-1.700	-0.58	O	-3.032	1.883	-1.720	-0.64
43	O	-0.786	2.536	-2.959	-0.58	O	-0.765	2.548	-2.937	-0.64
44	O	-1.377	3.677	-0.624	-0.58	O	-1.398	3.658	-0.608	-0.64
45	O	-2.170	-2.586	2.102	-0.58	O	-2.140	-2.594	2.095	-0.64
46	O	-1.385	-3.723	-0.177	-0.58	O	-1.394	-3.704	-0.201	-0.64
47	O	2.160	-2.562	-2.139	-0.58	O	2.167	-2.563	-2.107	-0.64
48	O	3.780	-0.862	-0.879	-0.58	O	3.772	-0.831	-0.888	-0.64
49	O	2.695	0.967	2.757	-0.58	O	2.686	0.937	2.761	-0.64
50	O	0.456	0.146	3.947	-0.58	O	0.432	0.163	3.936	-0.64
51	O	1.105	-3.209	0.350	-0.60	O	1.132	-3.208	0.348	-0.68
52	O	2.735	-1.467	1.420	-0.60	O	2.730	-1.468	1.447	-0.68
53	O	0.510	-2.098	2.643	-0.60	O	0.505	-2.124	2.633	-0.68

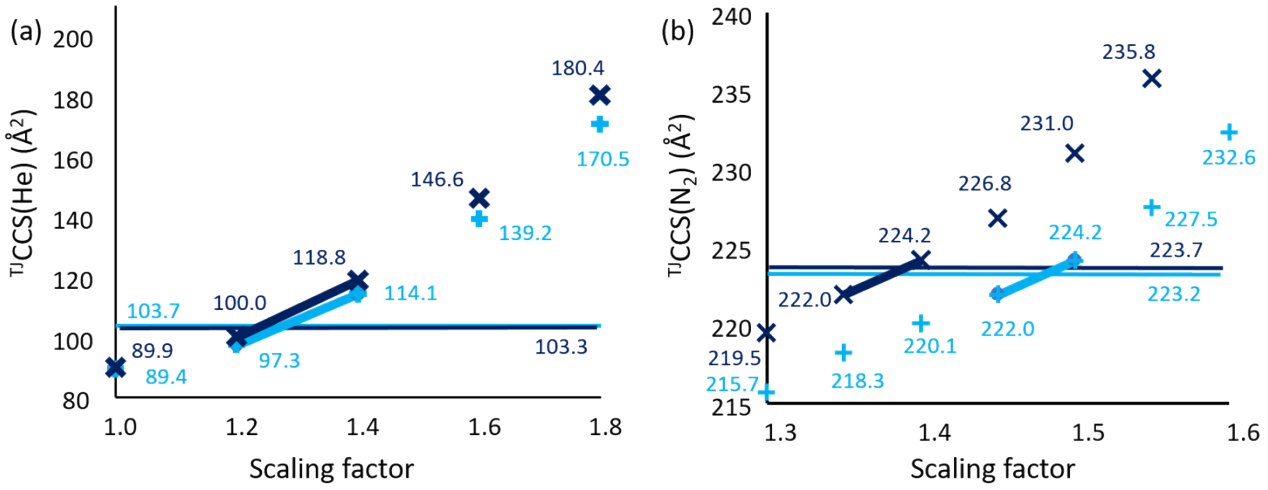

Figure S23. (a) Collision cross sections calculated with the trajectory method for Lindqvist anions (a) in helium and (b) in N_2 using Universal Force Field Lennard Jones ε and σ parameters for Mo or W multiplied by different scaling factors. The data in light blue represents data obtained for $Mo_6O_{19}^{2-}$ and in dark blue $W_6O_{19}^{2-}$. The horizontal lines represent the targeted experimental ^{DT}CCS values in He and N_2. The chosen scaling factors were interpolated with linear functions between the two closest scaling factors, as shown.

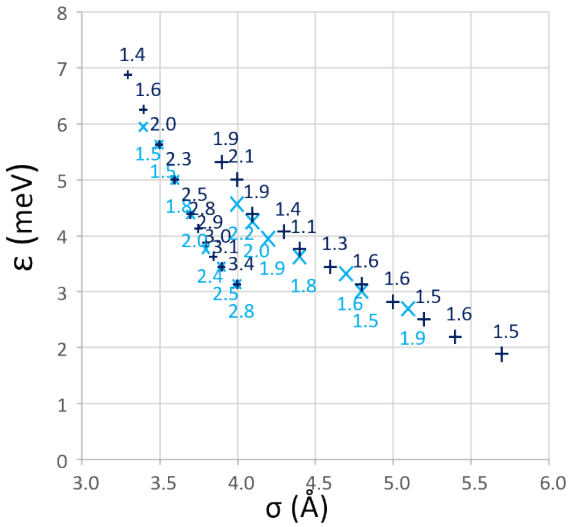

Figure S24. Points of minimal relative error on the LJ parameters surface: Mo-He data in small light blue diagonal crosses, W-He data in small dark blue vertical crosses, Mo-N_2 data in large light blue diagonal crosses, W-N_2 data in large dark blue vertical crosses. Light blue labels for Mo-He and Mo-N_2 data placed below each point is the accumulated relative error in percentage. Dark blue labels for W-He and W-N_2 placed above each point is the accumulated relative error in percentage.